Metals & corrosion

Effect of pre-compression on microstructural evolution, mechanical property and strengthening mechanism of AZ31 alloy

Xinfeng Li[1] and Qizhen Li[2,*]

[1] *Sino-French Institute of Nuclear Engineering and Technology, Sun Yat-sen University, Zhuhai 519082, Guangdong, China*
[2] *School of Mechanical and Materials Engineering, Washington State University, Pullman 99164, USA*

ABSTRACT

The effect of pre-compression deformation on the microstructural evolution, mechanical property and deformation behavior of AZ31 magnesium alloy was studied. The alloy was microstructurally characterized with a combination of optical microscopy, electron backscatter diffraction, X-ray diffraction and energy-dispersive spectrometer. The results indicate that average number of twins per grain and dislocation density increases with an increase in compressive pre-deformation level. Stress–strain curves of low pre-strained samples (0%, 1% and 3%) present concave-up features, whereas concave-down shapes are detected for high pre-strained samples (6% and 8%) in uniaxial compression tests. The corresponding underlying deformation mechanism transists from a twin-dominated mechanism to a slip-dominated mechanism. This deformation mechanism transition is related to {10–12} twinning, which leads to grain refinement and crystal orientation change, as well as increased dislocation density. The yield strength linearly increases with increasing equivalent grain size regardless of the deformation mechanisms. Quantitative analysis reveals that the contributions from texture strengthening, twinning/grain boundary strengthening and dislocation strengthening increase as pre-compression level increases. Texture strengthening is the dominant strengthening mechanism for high pre-strained samples.

Introduction

Magnesium (Mg) and its alloys are attractive structural materials in the automotive and railway industries due to their low density, good machinability and high specific strength [1–4]. These alloys possess, however, only limited plasticity and a noticeable mechanical anisotropy derived from their hexagonal close packed (HCP) structure with particular plastic deformation mechanisms [5]. The plastic deformation patterns of Mg alloys can include slip deformation and twinning deformation that co-occur

Springer

[6, 7]. Slip systems of Mg alloys contain basal, prismatic and pyramidal plane slip along the $a/3\langle 11\text{-}20\rangle$ direction ($\langle a\rangle$), prismatic plane slip along the $\langle 0001\rangle$ direction ($\langle c\rangle$) and pyramidal plane slip along the $a/3\langle \text{-}2113\rangle$ direction ($\langle c+a\rangle$) [8], as schematically shown in Fig. 1a–f. The critical resolved shear stresses (CRSSs) of various slip systems are significantly different. At room temperature, the CRSS of a non-basal slip of pure Mg is approximately 50 MPa, whereas the value of CRSS is about 0.52 MPa for basal slip, indicating that basal plane slip deformation of Mg is easily activated. The basal plane slip only offers two independent slip modes, which cannot meet the von Mises criterion that requires at least five independent slip systems to generate homogenous deformation for polycrystalline metals [9]. Accordingly, Mg alloys exhibit poor ductility due to limit dislocation slips. Twins also play a significant role in the plastic deformation behavior of pure Mg and its alloys. Twinning modes involve {10–12} tension twins, {10–11} contraction twins and {10–11}–{10–12} double twins [10]. Because the ratio of c/a in Mg is 1.624,

{10–12} tension twins are the dominant twin system in the alloy, which can be generated via a changed loading direction in terms of crystal orientation, i.e., the compressive stress direction perpendicular to the c-axis direction or tensile stress direction along the c-axis direction. As tension twins occur, twin lattice rotates 86.3° relative to matrix lattice (Fig. 1g). This leads to a preferred grain orientation, and consequently anisotropic mechanical properties of the alloys.

The dominant deformation mechanism depends on the Mg alloy grain size [6, 11–14]. As grain size increases, the transition from slip deformation to twin deformation takes place, and corresponding critical grain sizes for pure Mg or Mg alloys have been determined. Li et al. [12] revealed that twinning was suppressed in fine-grained pure Mg, and that the twinning deformation mechanism dominated as the alloy grain size exceeded 2.7 μm. This was also theoretically validated by Fan et al. [11]. Choi et al. [14] indicated a deformation mechanism transition as grain size of hot extrusion pure Mg was of 1 μm. The

Figure 1 Schematic illustration of **a**–**f** slip deformation and **g** tension twin deformation of magnesium alloys.
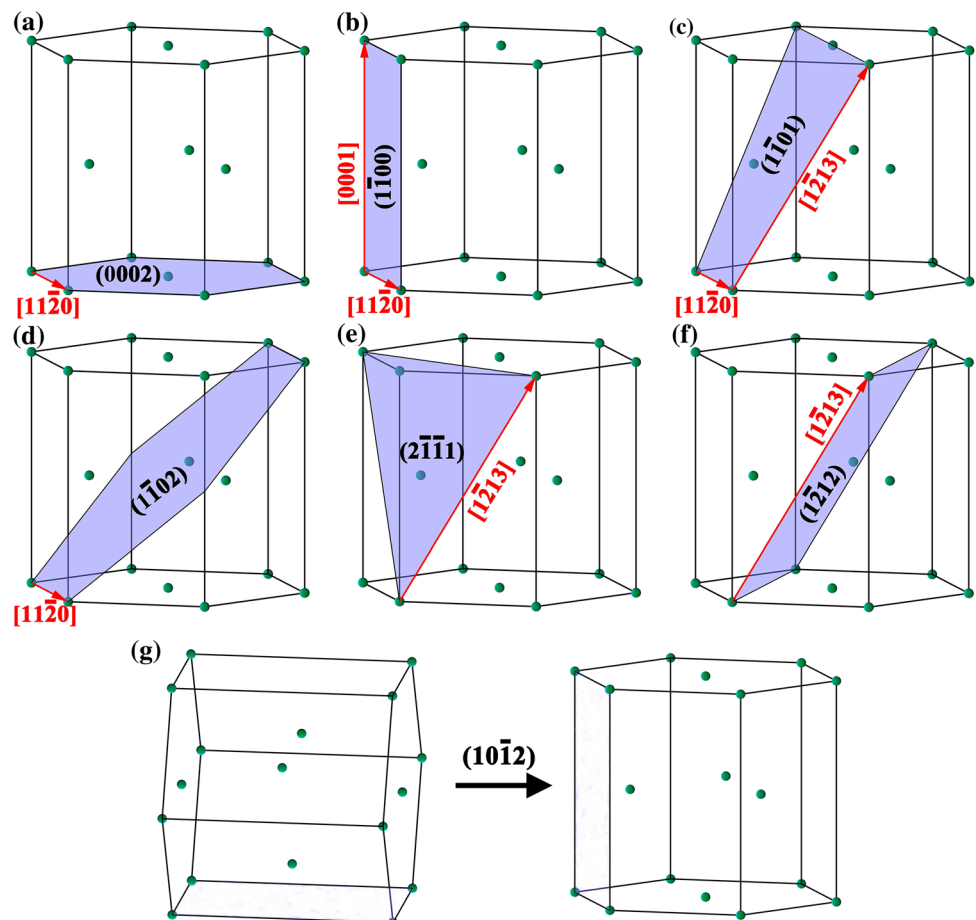
critical grain size was 3 to 4 μm for ZK60 Mg alloy [15] and 8 μm for the AZ31 Mg alloy [16]. Several explanations on deformation mechanism transition related to grain size has been proposed. Cepeda-Jimenez et al. [6] argued that as grain size of pure Mg was reduced from 19 to 5 μm, a transition from twinning-dominated deformation to slip-dominated deformation took place, which was attributed to fine-grained Mg with high grain connectivity favoring basal slip. The CRSS ratio of non-basal slip to basal slip reduced with decreasing grain size, which was in favor of non-basal slip [7]. The activation of twinning stresses increased more rapidly than that of slip with a decrease in grain size. A critical grain size, below which slip mechanism governed the deformation, was eventually reached, according to Meyers et al. [17].

Analogous to grain boundaries of Mg alloys, twinning lamellae can subdivide grains, resulting in grain refinement [18, 19]. In comparison with grain boundaries, twin boundaries always show higher mechanical and thermal stability [20]. Previous investigation has focused on the influence of grain refinement through twin boundaries on mechanical properties of Mg alloys, including tensile properties [18, 21–25], compressive properties [5, 22, 26], fatigue properties [22, 27], stretch formability [28–30] and hardness [31]. However, studies on the underlying deformation mechanism and strength mechanism of these alloys have been limited. This study sheds light on the compressive mechanical response, deformation behavior and strengthening mechanism of AZ31 alloy refined by twin lamellae. To introduce different twinning fractions in the tested alloy, pre-compression tests with various strain levels were conducted. These samples were subsequently reloaded at room temperature until they fractured. The corresponding mechanical properties of the samples were evaluated. The strengthening mechanism of twin-refined alloys with various pre-deformation levels was quantitatively discussed.

Materials and experimental methods

The material employed in the present study was a commercial AZ31 Mg alloy, which was received in the form of extruded bars with a diameter of 10 mm. These bars were annealed at 400° for 4 h. Afterward, two groups of bars were pre-compressed along

extrusion direction (ED) with various pre-compression levels of 0%, 1%, 3%, 6% and 8%, designated as 0P, 1P, 3P, 6P and 8P samples. The first group of specimens was prepared to characterize their microstructural evolution using optical microscopy (OM), electron backscatter diffraction (EBSD) and X-ray diffraction (XRD). The second group of samples was used to fabricate compressive samples with a diameter of 10 mm and a height of 11.6 mm. These samples were recompressed along ED with a nominal strain rate of 7×10^{-5} s^{-1} using a universal testing machine (Instron 8801) [2]. For 0P, 3P and 6P samples, the compressive tests were repeated three times, whereas 1P and 8P samples were compressed one time.

Following standard preparation procedures of metallographic samples, representative samples were ground and then mechanically polished to investigate their microstructure. The samples were etched in the solution, which consisted of 4.2 g picric acid, 90 ml alcohol, 10 ml acetic acid and 10 ml deionized water for 90 s, and then observed by OM (Zeiss Axio Scope). On the basis of OM images, about 100-250 grains with 600-1200 twins on the whole cross section were randomly selected and statistically analyzed to obtain the average number of twin in per grain (ANTPG) and the average length of per twin (ALPT) of pre-compressed samples, which can be expressed as:

$$\mathrm{ANTPG} = \sum_{1}^{i} N_T \Big/ i \tag{1}$$

$$\mathrm{ALPT} = \sum_{1}^{i} G \sum_{1}^{j} L_T \Big/ \sum_{1}^{i} N_T \tag{2}$$

where i was the number of grains. N_T was the number of twins in i_{th} grain. G was the grain. j was the number of twins in i_{th} grain. L_T was the length of specific twin. In addition, XRD was performed with scanning range from 20° to 80°. The dislocation density of samples is estimated according to the modified Williamson-Hall method [32]:

$$\Delta K = 0.9/D + (\pi M^2 b^2/2)^{1/2} \rho^{1/2} (K\overline{C}^{1/2}) + O(K^2\overline{C}) \tag{3}$$

where $K = 2\sin\theta/\lambda$, $\Delta K = 2\cos\theta\Delta\theta/\lambda$, θ and λ are diffraction angle and incident ray wavelength, D is a size parameter, M is a constant replying on the effective outer cut-off radius of dislocations, b is the

magnitude of the Burgers vector of dislocation, ρ is the dislocation density, O is a non-interpreted high-order terms in $K^2\overline{C}$, which is not considered, $\overline{C}$ is the average contrast factors of dislocation. The value of $\overline{C}$ for Mg alloys with HCP structure is calculated by [33]:

$$\bar{C}_{hkl} = \bar{C}_{hk0}(1 + q_1 x + q_2 x^2) \tag{4}$$

where $x = (2/3)(l/ga)^2$, l and a are the lattice constants for Mg crystal, g is the magnitude of the diffraction vector. $\bar{C}_{hk0}$, q_1 and q_2 are related coefficients obtained in the Ref. [34]. The dislocation density of the alloys can be evaluated by the following equation:

$$\rho = 2m^2 / \pi M^2 b^2 \tag{5}$$

After conventional mechanical polishing, electro-polishing tests followed in AC2 solution at a voltage of 15 V for 15 s to prepare EBSD samples. The observation section of EBSD samples was perpendicular to the direction of extrusion. EBSD analysis was performed on JEOL JSM-7800F scanning electron microscopy and a HKL-EBSD system with a step size of 0.5 μm. For XRD analysis, an X-ray diffractometer with a Cu target was operated at 40 kV to observe the transverse cross-sectional plane. The scanning rate and the step size were 6° min^{-1} and 0.02°, respectively. The macrotexture of the samples was characterized by Rigaku D/MAX-2500 XRD at 45 kV with the tilt angle of samples from 0° to 80°.

Results

Twinning and texture of pre-compressed AZ31 alloys

Figure 2 shows light optical microstructure images of AZ31 alloys with different pre-compression levels to reveal the evolution of twin features. The as-received sample exhibits equiaxed grains with an average grain size of 120 ± 40 μm, which is determined by the linear intercept method (Fig. 2a). Magnified images in Fig. 2a′–a″ reveal that the sample is free of twinning. Twinning is introduced within the grains (Fig. 2b–d″) when pre-compression tests are performed. Some grains of the 3P sample show distinct twinning features within the grains, and others lack of twinning (Fig. 2b). Most of twinning parallels each

other within a specific grain attributed to the fact that pairs of twin variants with higher Schmid factor are preferentially activated during pre-compression compared with other twin variants [35]. At the higher pre-compression levels of 6% and 8%, parallel twinning morphology of 6P and 8P samples still dominates, as seen in Fig. 2c–c″, d–d″, respectively, which is similar to that of the 3P sample. The difference between 3P, 6P and 8P samples is the amount of twinning per grain and twinned grain fraction. To quantify twinning features accurately, histograms of twin number per grain and twin length of 3%, 6% and 8% pre-compressed samples are statistically established in Fig. 3, indicating that these histograms basically follow a normal distribution. The ratio of the number of un-twinned grains to the total number of grains decreases with increasing pre-compression level, i.e., 22%, 16% and 10%, for the 3P, 6P and 8P samples, respectively. According to Eq. (1) and Eq. (2), the values of ANTPG and ALPT are 3 and 122 μm, 5 and 142 μm, 9 and 111 μm for 3P, 6P and 8P samples, respectively. The value of ANTPG gradually increases with higher compressive strain, whereas the value of ALPT first increases, and then decreases after it reaches the peak value at 6P sample. EBSD and XRD tests, which can be used to characterize microscopic and macroscopic texture evolution, were conducted to clarify the category of these parallel twinning. Figure 4a–d shows inverse pole figures of samples from EBSD tests, indicating that compressive pre-deformation leads to twinning. The distribution of twins is uneven, i.e., some grains are enriched with twins, whereas others are free of twins (Fig. 2). Fewer twins are detected in the 8P sample (Fig. 4d) compared with 3P and 6P samples (Fig. 4b, c) due to the selected areas. For the {0002} XRD pole figures, the 0P sample exhibits a relatively random distribution with several discrete local maxima. Some maxima are distributed within the ring of 60° to 90° relative to ED (Fig. 4a′). The maximum pole value gathers at the center of the pole figures (Fig. 4b′–d′) as strain level increases, indicating a preferred orientation in the samples. The {10–10} pole figures show an opposite trend with increasing strain level, as given in Fig. 4b″–d″. Based on XRD pole figures and previous studies [10, 23, 26, 35], it is demonstrated that parallel twinning is mainly {10–12} extension twinning.
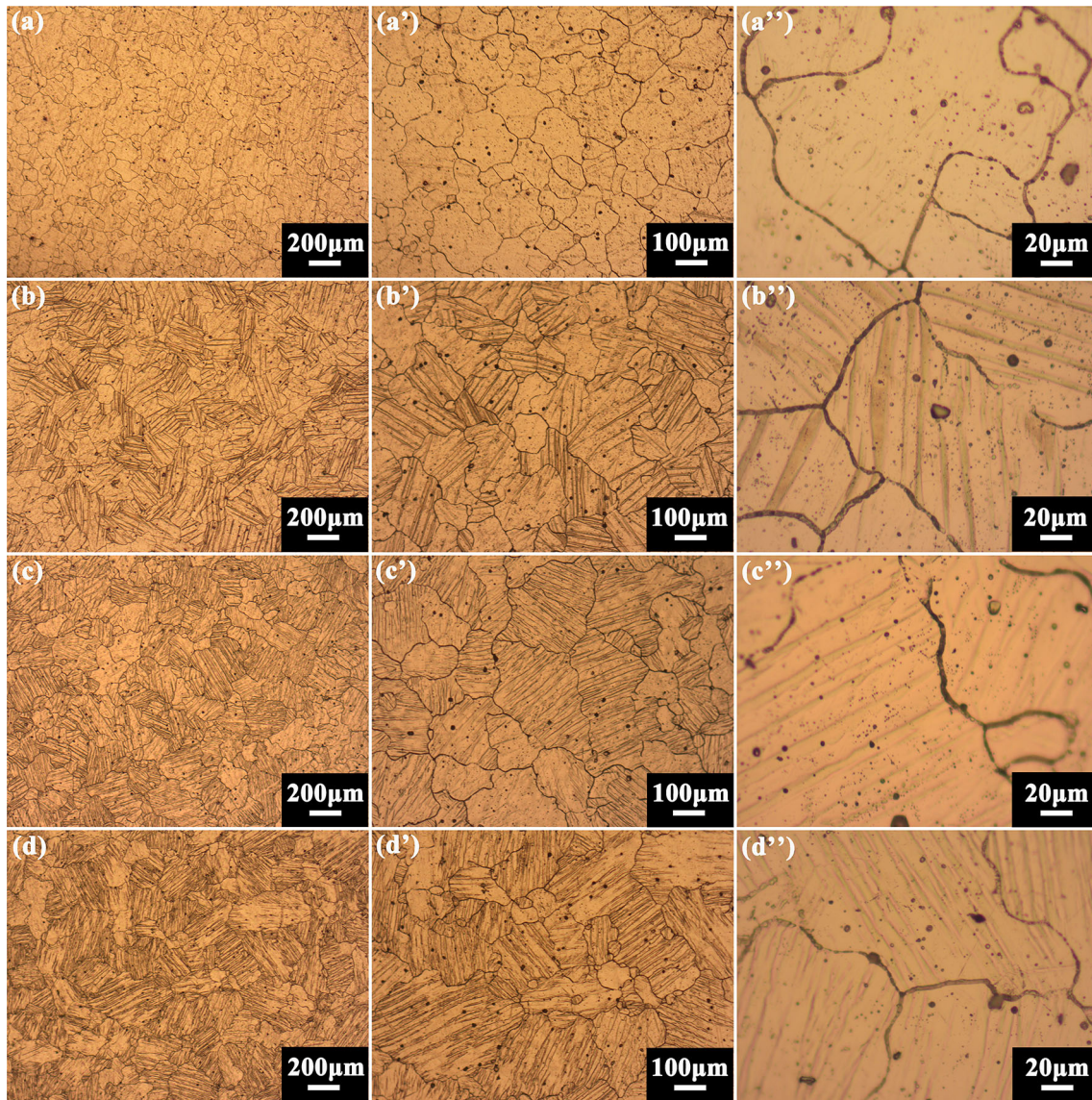
Figure 2 Optical microscopy images of AZ31 Mg alloy with various pre-compression levels in increased magnification **a**, **a″** 0P; **b**, **b″** 3P; **c**, **c″** 6P; **d** and **d–d″** 8P.

Dislocation density and precipitates of pre-compression AZ31 alloys

Figure 5 presents XRD patterns of samples with various pre-compression levels, indicating that the alloys consist of a single α-Mg phase with a P63/mmc space group in comparison with the result of PDF-#35-0821. Careful observation shows that the height of the (10-10) peak decreases, and the height of the (0002) peak increases gradually with increasing strain level. The relatively integrated intensity ratio of $I_{(0002)}/I_{(10-10)}$ reflecting a preferential orientation of the alloys [36, 37] is 0.04 for 0P sample, 0.18 for 3P

sample, 2.12 for 6P sample and 6.99 for 8P sample. An increase in $I_{(0002)}/I_{(10-10)}$ ratio implies an increasing orientation of the (0002) plane parallel to the scanning surface. This result is consistent with the XRD pole figures. Additionally, dislocation density of the samples was evaluated based on the modified Williamson-Hall method and corresponding results are listed in Table 1. The calculated dislocation density is about 9.58×10^{12} m^{-2} in the as-received sample, which is comparable to that of Mg-2wt. %Al sample (about 1.12×10^{13} m^{-2}) [8]. The dislocation density is 3.13×10^{13} m^{-2}, 4.33×10^{13} m^{-2}, and 5.51×10^{13} m^{-2} as pre-strain increases from 3%, to 6%, and to
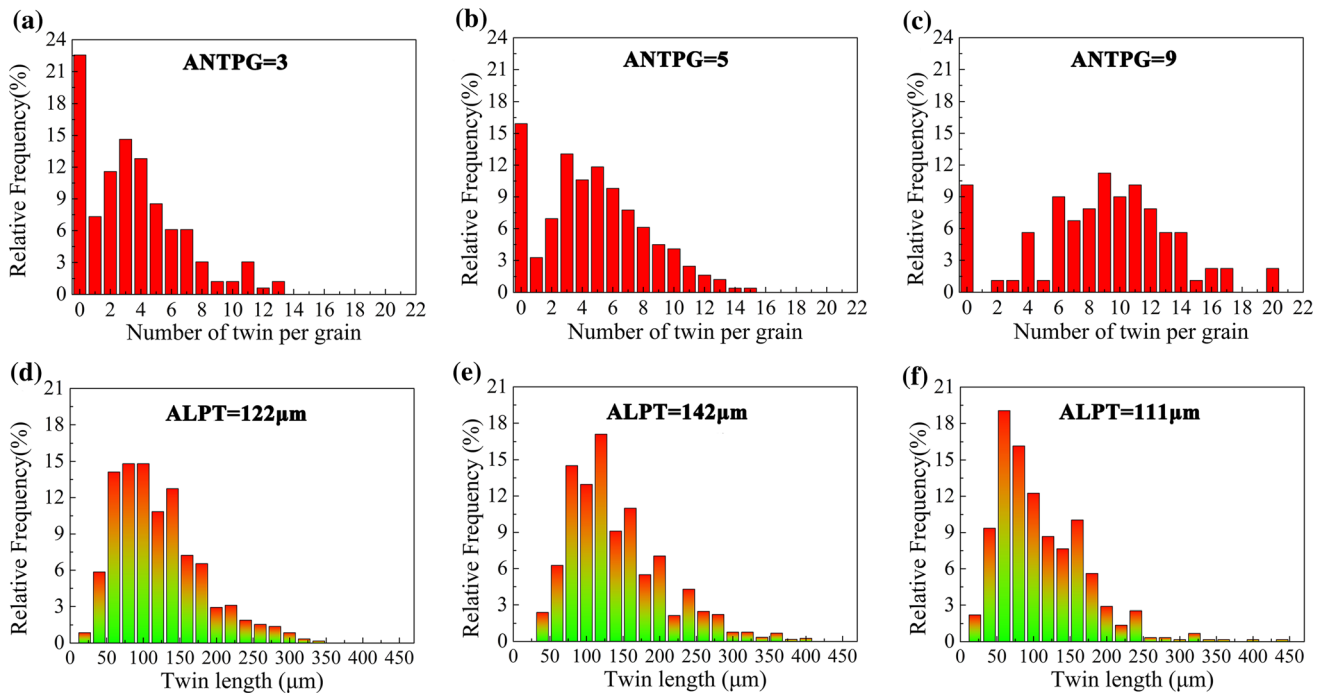
**Figure 3** Histograms of number of twin per grain (**a**–**c**) and twin length (**d**–**f**) of pre-compressed AZ31 alloy. **a**, **d** 3P; **b**, **e** 6P; **c**, **f** 8P. ANTPG: average number of twin in per grain. ALPT: average length of per twin.

8%, respectively. Figure 6 presents precipitates in the alloy and the alloys are composed of two types of precipitates. The chemical composition of one precipitate consists of Al and Mn elements and the other precipitate is made up of Si elements.

Compressive mechanical properties of pre-compression AZ31 alloys

Representative stress–strain curves of samples with various pre-compression levels are presented in Fig. 7a. As the pre-strain level increases, the plasticity of samples dramatically decreases, and the maximum stress is slightly reduced. Interestingly, two types of curve appearances are observed, depending on pre-compression levels. A quadratic polynomial fitting on the curve was conducted [38] to classify the curve shapes. According to the results of this polynomial second differential, the curves with concave-up $(d^2\sigma/d\varepsilon^2 > 0)$ or concave-down $(d^2\sigma/d\varepsilon^2 < 0)$ profiles are determined. For 0P, 1P and 3P samples, designated as low pre-strained samples, the curves exhibit concave-up characteristics. The degree of concave-up of the stress–strain curve decreases with an increase in the pre-strain level. By

contrast, 6P and 8P samples, designated as high pre-strained samples, appear concave-down appearances, which is similar to the tensile stress–strain curve shape of the AZ31 alloy at room temperature marked by an open star in purple color in Fig. 7a [10]. Figure 7b presents the relation between work hardening rate and strain taken from corresponding stress–strain curves. The work hardening rate dramatically decreases at first for low pre-strained samples, then increases and finally decreases again with increasing strain, whereas it exhibits sharp hardening decrease and then presents a relatively slow decrease rate for high pre-strained samples. This change in the hardening rate of high pre-strained samples correlates with an elastoplastic transition [7]. Compressive mechanical parameters obtained from stress–strain curves are illustrated in Fig. 7c–e. The values of yield strength pronouncedly increase as strain level increases, i.e., 97 MPa for 0P, 121 MPa for 1P, 155 MPa for 3P, 225 MPa for 6P and 280 MPa for 8P samples. Peak strength and fracture strain show simultaneously a decreasing trend, at 394 MPa and 13.49% for 0P, 390 MPa and 12.77% for 1P, 389 MPa and 12.60% for 3P, 369 MPa and 9.22% for 6P, and 362 MPa and 5.23% for 8P samples,
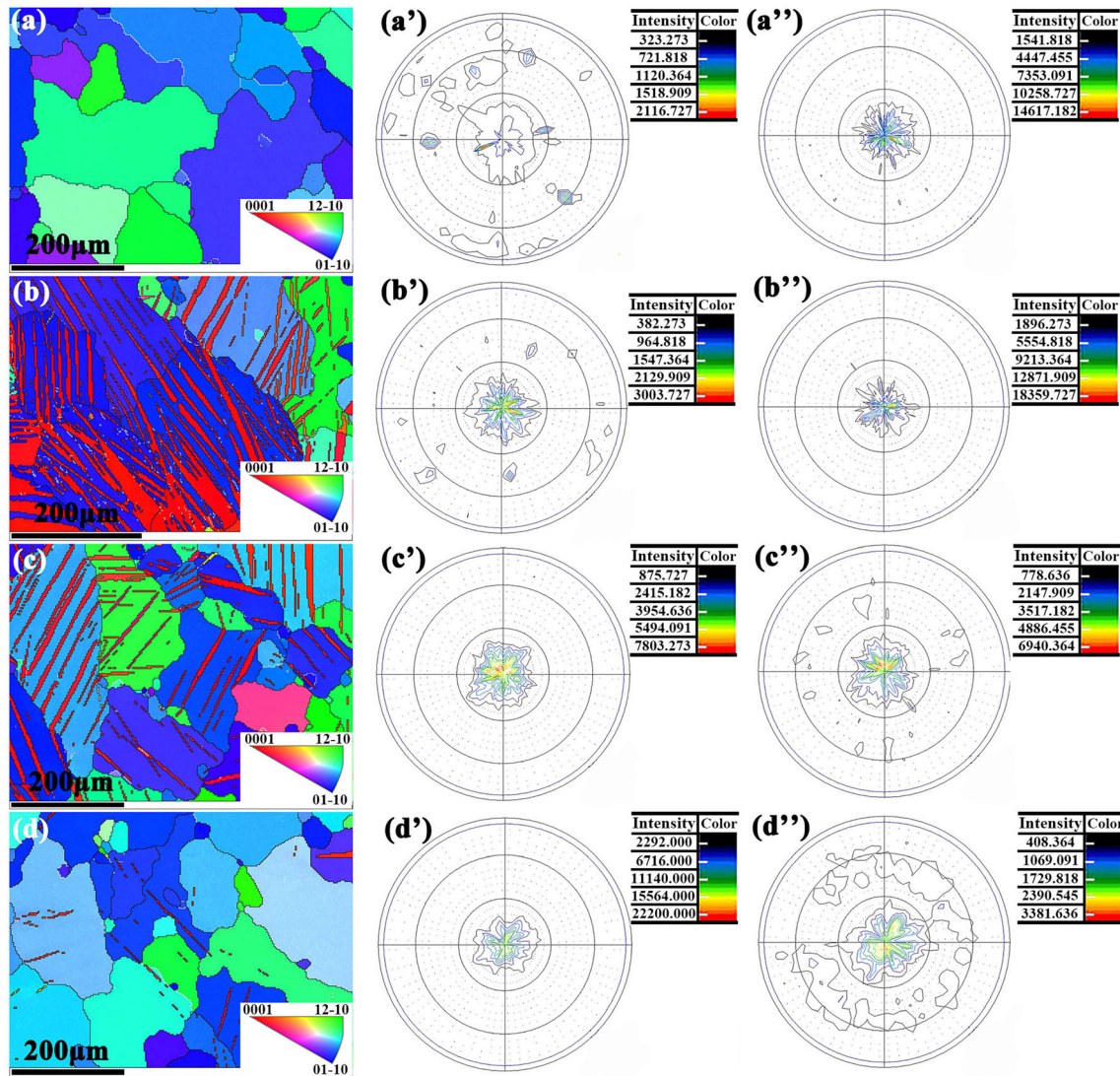
Figure 4 EBSD and XRD pole figures of samples with various strain levels **a**, **a″** 0P; **b**, **b″** 3P; **c**, **c″** 6P and **d**, **d″** 8P. **a**–**d** inverse pole figures; **a′**–**d′** {0002} pole figures; **a″**–**d″** {10-10} pole figures.

respectively. Figure 8 summarizes the relationship between yield strength and pre-compression level of AZ31 alloy, indicating that an increase in pre-compression level correlates with increasing yield strength due to grain refinement by {10–12} twins [4, 19, 23, 26, 27, 37]. Their quantitative relationship can be described as follows:

$$\text{Yield strength} = 96.78 + 17.03\,\text{pre - compression} \tag{6}$$

Discussion

Deformation mechanism transition of pre-compression AZ31 alloys

According to Fig. 7a, compressive stress–strain curve appearances transition from concave-up shape to concave-down shape with an increase in pre-compression level. This differs from the previous study results from Xin et al. [26] and Song et al. [23], who indicated that all stress–strain curves of pre-deformation AZ31 samples show a concave-up shape. The discrepancy between previous studies [23, 26] and the present work may be attributed to compressive strain level, loading direction, and grain size. Stress–
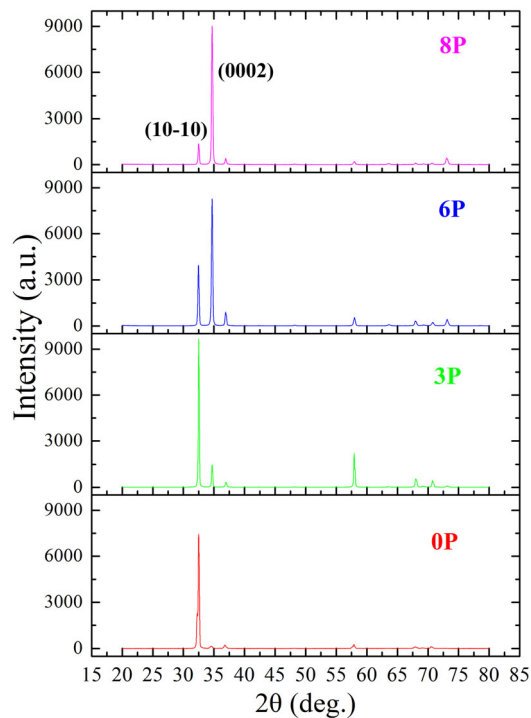
Figure 5 XRD pattern of AZ31 samples with various pre-compression levels.

strain curves with concave-up shape in previous studies [2, 12, 13, 39, 40] are dominated by twinning deformation, especially {10–12} twinning. Slip deformation serves as the dominant mechanism for the concave-down feature of stress–strain curves [5, 6, 13, 18]. Accordingly, it is concluded that increasing pre-compression level leads to the transition of the dominant deformation mechanism.

With an increasing pre-compression level, the deformation mechanism transitions from twin- to slip-dominated. This transition can be related to the formation of {10–12} twinning and dislocation density. The deformation mechanism of Mg alloys depends on grain size [11, 12, 14–16], as mentioned in Introduction part. Twin deformation prevails when the alloy grain size exceeds its critical value. Below that value, slip deformation dominates. After pre-compression deformation, parallel {10–12} twins are formed, leading to grain refinement by twinning lamellae [18]. The degree of grain refinement enhances with increasing strain due to increased

twinning, as seen in Fig. 3. Finer grain yields higher grain/twin boundary connectivity, which favors slip transfer across these boundaries, and the strain of samples with finer grain is primarily accommodated by slip deformation [6]. Moreover, {10–12} twin lamellae change crystal orientation of parent grains, resulting in the *c*-axis direction of twinned grains almost parallel to the compressive stress direction. The parent and twinned grains correspond to different deformation mechanisms as the compression direction is along ED. For parent grains, twinning deformation dominates because the compressive direction is almost perpendicular to their *c*-axis direction [35], whereas twinned grains with their *c*-axis direction parallel to compression direction are controlled by slip deformation. It was reported by Xie et al. [41], Syed et al. [42], and Byer et al. [43] that the prevalence of pyramidal slips was detected as single-crystal Mg was compressively loaded along the [0001] *c*-axis direction. As seen from Fig. 3, an increase in strain accompanies with increasing twinned grain fraction so that the transition of deformation mechanism occurs. Increasing pre-compression level corresponds to an increase in dislocation density (Table 1), which preferentially facilitates prismatic slip over the basal slip. Hutchinson et al. [44] revealed that when dislocation density varied from 10^6 to 10^{14} m^{-2}, shear stress ratio between prismatic slip and basal slip dropped from 40:1 to 2:1. Accordingly, an increasing dislocation density of high pre-strained samples enhances non-basal slip activity accompanied with deformation mechanism transition.

Strength mechanism of pre-compression AZ31 alloys

The effect of grain size on the compressive yield strength of pure Mg or Mg alloys with different deformation mechanisms has been investigated, and their relationship are divided into two cases, as shown in Fig. 9. Case 1) The yield strength first increases, reaches the peak value and then decreases [11, 12, 14, 38]; Case 2) The yield strength always increases with two slopes [38]. Fine grain samples

Table 1 Dislocation density of AZ31 samples with different pre-compression levels	Strain level	0%	3%	6%	8%
	Dislocation density (m^{-2})	9.58×10^{12}	3.13×10^{13}	4.33×10^{13}	5.51×10^{13}
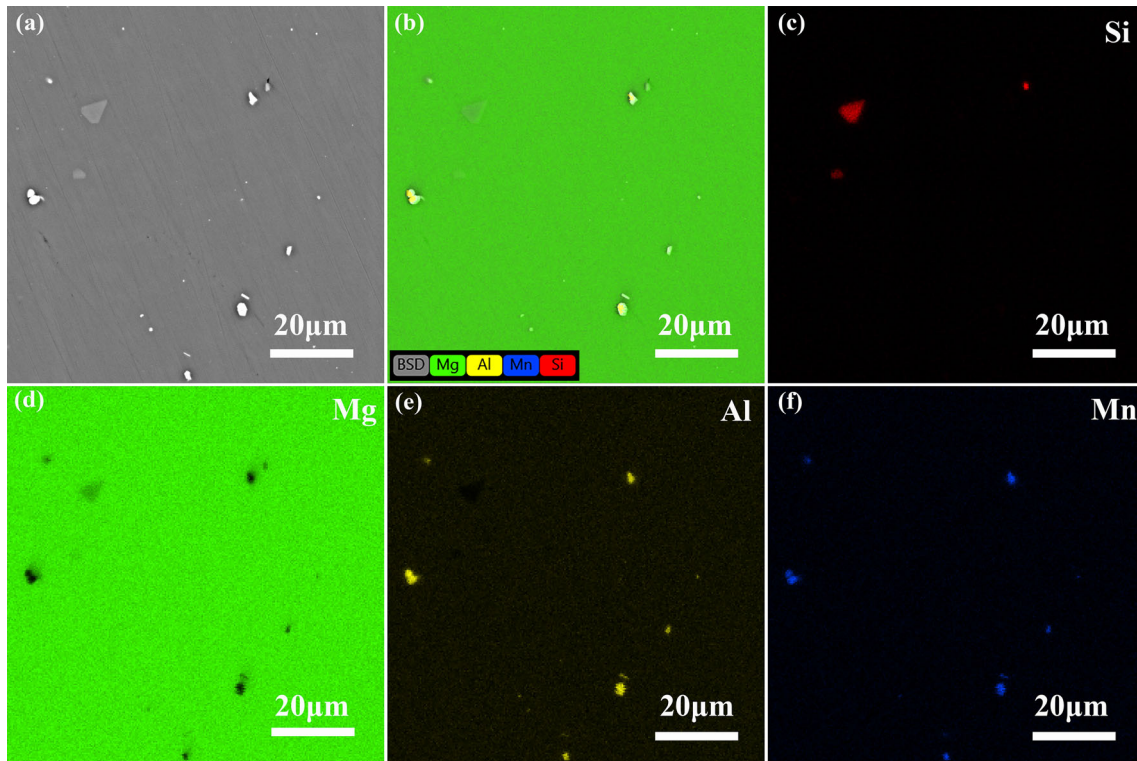
Figure 6 EDS results of two types of precipitates. **a, b** overview of precipitates; **c** Si element; **d** Mg element; **e** Al element and **f** Mn element.

enhance twin activation stress due to higher Schmid factor and then suppress the formation of twinning compared with coarse grain samples [2, 35] for twin-dominated compressive deformation (open shape in Fig. 9). This leads to an increased yield strength with decreasing grain size. The alloys with slip-dominated deformation exhibit inverse Hall–Petch relationship, when the grain size is further reduced, which is related to grain rotation or grain boundary sliding [14]. In order to quantify the relation between yield strength and grain size in the present study, equivalent grain size (d_E) of the samples are defined as [14]:

$$d_E = d/\text{ANTPG} \tag{7}$$

According to Eq. (7), the values of d_E of the samples are calculated and listed in Table 2. Corresponding relation between yield strength and equivalent grain size marked by down triangle is presented in Fig. 9. Yield strength of alloys linearly increases as grain size reduces regardless of dominant deformation mechanism. This result is not consistent with the results from previous research [12, 14, 38] (Fig. 9). Yield strength (σ_s) of 0P AZ31 alloys can be enhanced by pure Mg (σ_{mg}), grain

boundary strengthening ($\Delta\sigma_{gb}$), dislocation strengthening ($\Delta\sigma_{ds}$) and other strengthening ($\Delta\sigma_{\text{other}}$) including solid solution strengthening ($\Delta\sigma_{ss}$) and precipitation strengthening ($\Delta\sigma_{ps}$), which can be written as:

$$\sigma_s = \sigma_{mg} + \Delta\sigma_{gb} + \Delta\sigma_{ds} + \Delta\sigma_{\text{other}} \tag{8}$$

$$\Delta\sigma_{\text{other}} = \Delta\sigma_{ss} + \Delta\sigma_{ps} \tag{9}$$

The value of σ_{mg} about 13 MPa is selected based on the work from Li et al. [12]. The contribution of grain boundary strengthening can be approximated according to Hall–Petch law expressed as [45]:

$$\Delta\sigma_{gb} = k/d^{1/2} \tag{10}$$

where k is a constant and d is the grain size of the 0P sample. The value of $\Delta\sigma_{gb}$ is about 25 MPa when one inserts the value of $k = 269$ MPa $\mu\text{m}^{-1/2}$ [46] and $d = 120$ μm into the equation. Dislocation strength can then be estimated by Eq. 11 [3]:
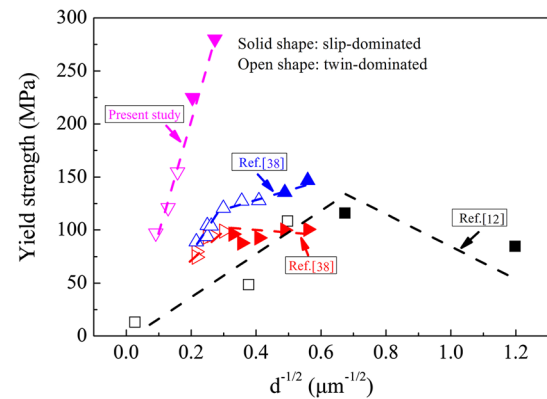
$$\Delta\sigma_{ds} = AMGb\sqrt{\rho} \tag{11}$$

where A is a constant that reflects dislocation interactions of magnesium ($A = 0.2$) [47]. M is the average orientation factor of magnesium ($M = 6.5$) [48]. G is

Figure 7 **a** Compressive stress–strain curves; **b** working hardening rate; **c** yield strength; **d** peak strength and **e** fracture strain of samples with various pre-compression levels. The data of tensile stress–strain curve of AZ31 alloy marked by open circles in purple color in (**a**) from Ref. [10].
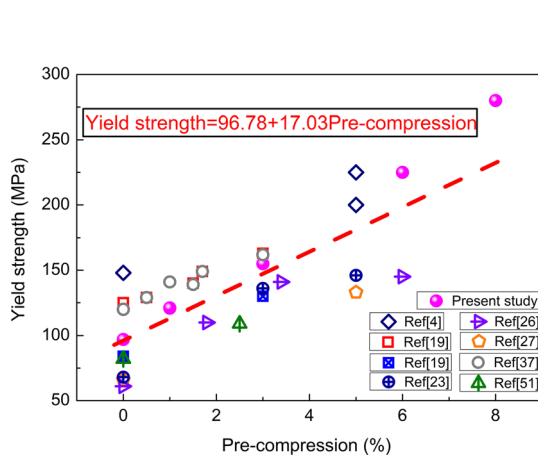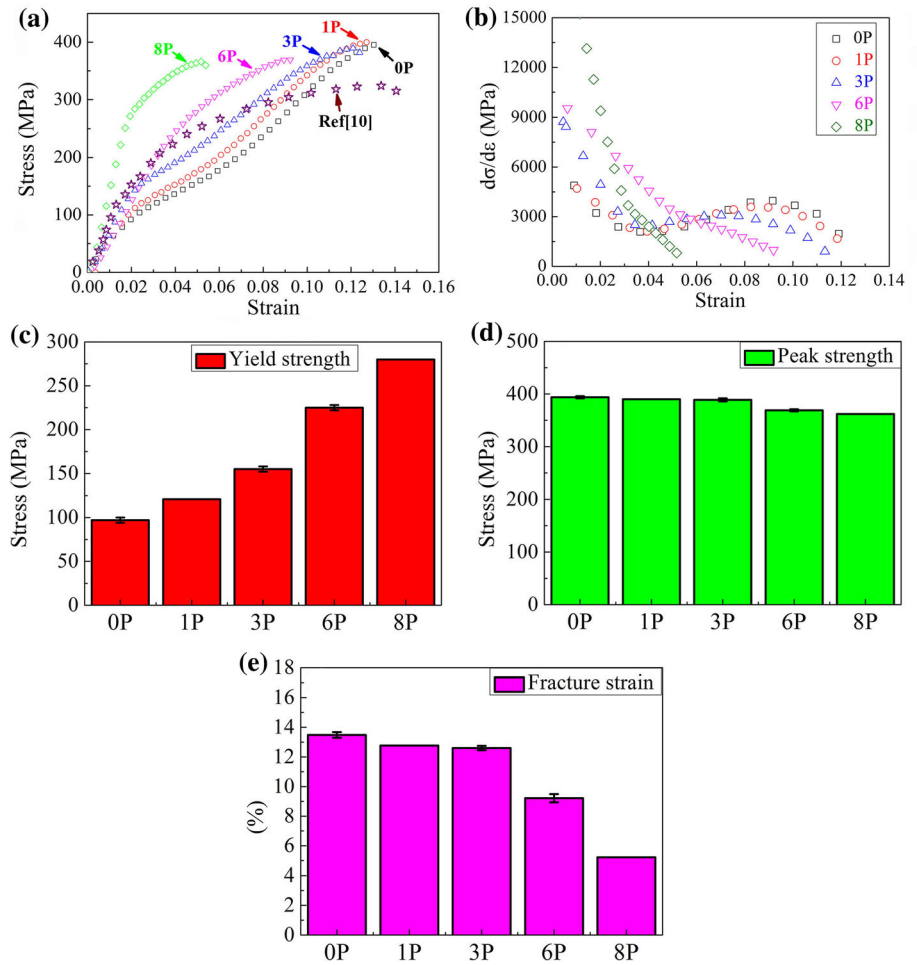
**Figure 8** Dependence of yield strength on pre-compression level of AZ31 alloy.

Figure 9 Dependence of yield strength related to slip-dominated deformation or twin-dominated deformation on the reciprocal of square root of grain size.

the shear modulus of magnesium ($G = 16.6$ GPa) [14]. b is Burgers vector ($b = 3.21 \times 10^{-10}$ m) [3] and ρ is

the dislocation density ($\rho = 9.58 \times 10^{12}$ m²). So the value of $\Delta\sigma_{ds}$ is 21 MPa. Based on the experimental yield strength of 0P sample (97 MPa) and Eq. (4), the value of $\Delta\sigma_{other}$ is 38 MPa.

Table 2 Equivalent grain size of AZ31 samples with different pre-compression levels

Strain level	0%	3%	6%	8%
Equivalent grain size (μm)	120	40	24	13
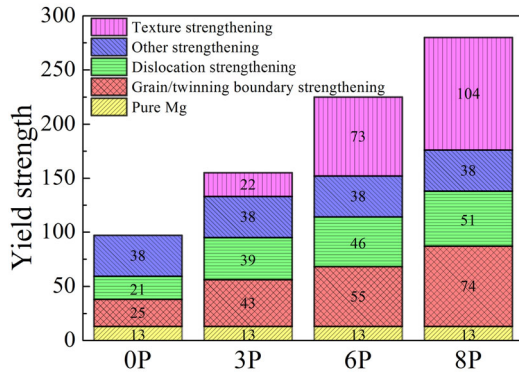
Figure 10 Respective contributions of pure Mg, grain/twin boundary strengthening, dislocation strengthening, other strengthening (solution strengthening and precipitate strengthening) and texture strengthening to yield strength of AZ31 alloys without and with pre-compressive deformation.

For rod magnesium alloy, {10–12} twinning and basal slip show relatively lower CRSS than those of other deformation mechanisms at room temperature as the compressive direction is parallel to the extruded direction. After pre-compression, the alloys exhibit a preferred orientation with the c axis direction aligned in ED. This can improve the yield strength of the alloy due to a low Schmid factor for {10–12} twins, and it correlates with another strengthening mechanism, i.e., texture strengthening ($\Delta\sigma_{ts-p}$) [49–51]. Accordingly, the total strength resources of pre-compression samples can be written as:

$$\sigma_{s-p} = \sigma_{mg-p} + \Delta\sigma_{gb-p} + \Delta\sigma_{ds-p} + \Delta\sigma_{other-p} + \Delta\sigma_{ts-p} \tag{12}$$

$$\Delta\sigma_{other-p} = \Delta\sigma_{ss-p} + \Delta\sigma_{ps-p} \tag{13}$$

The chemical composition and precipitates between 0P samples and pre-compression samples are the same, so the values of σ_{mg-p} and $\Delta\sigma_{other-p}$ are equivalent to those of σ_{mg} and $\Delta\sigma_{other}$, respectively. The value of $\Delta\sigma_{gb-p}$ is calculated with Eq. 14 [31]:

$$\Delta\sigma_{gb} = k \Big/ d_E^{1/2} \tag{14}$$

The value of $\Delta\sigma_{ds-p}$ is obtained with Eq. (11) and Table 1. Then $\Delta\sigma_{ts-p}$ is calculated using Eq. (12) combined with the experimental yield strength of pre-strained samples. The yield strength increment from various strengthening sources is summarized in Fig. 10. It is suggested that with an increase in strain level, the contribution from grain/twin boundary strengthening, dislocation strengthening and texture strengthening increases, particularly texture strengthening. Moreover, the 0P sample is mainly strengthened by $\Delta\sigma_{other}$, followed by $\Delta\sigma_{gb}$ and then $\Delta\sigma_{ds}$, whereas $\Delta\sigma_{ts-p}$ and $\Delta\sigma_{gb-p}$ act as dominant strengthening resources for the 6P and 8P samples.

Conclusions

(1) With an increase in pre-compression level from 0 to 3%, 6% and 8%, the average number of twin per grain of AZ31 alloys increases from 0 to 3, 5 and 9, and dislocation density increases from 9.58×10^{12} to 3.13×10^{13} m^{-2}, 4.33×10^{13} m^{-2} and 5.51×10^{13} m^{-2}, respectively.

(2) The shape of compressive stress–strain curve relies on the pre-strain level. The curves of the samples with low pre-strain exhibit concave-up features, whereas a concave-down appearance is observed for high pre-strain samples. Simultaneously, the corresponding deformation mechanism transits from twin- to slip-dominated mechanism. This transition can be explained in terms of grain refinement by twin lamellae and crystal orientation change due to {10–12} twins as well as increasing dislocation density.

(3) The yield strength of the alloys significantly increases, whereas peak strength and fracture strain decrease with an increasing compressive pre-strain level. Further strengthening mechanism analysis indicates that a combination effect of precipitate strengthening and solution strengthening acts as the dominant strengthening mechanism for the samples without pre-deformation. The high pre-strained samples are mainly strengthened by texture strengthening, followed by grain/twinning strengthening and then dislocation strengthening.

Funding

Compliance with ethical standards

Conflict of interest The authors declared that they have no conflicts of interest to this work.

References

[1] Li Q, Jiao X (2018) Exploration of equal channel angular pressing routes for efficiently achieving ultrafine microstructure in magnesium. Mater Sci Eng A 733:179–189

[2] Li X, Zhang J, Hou D, Li Q (2018) Compressive deformation and fracture behaviors of AZ31 magnesium alloys with equiaxed grains and bimodal grains. Mater Sci Eng A 729:466–476

[3] Han B, Dunand D (2000) Microstructure and mechanical properties of magnesium containing high volume fractions of yttria dispersoids. Mater Sci Eng A 277:297–304

[4] Chen H, Liu T, Lu L, He J, Zhai Y (2015) Influence of pre-strain and heat treatment on subsequent deformation behavior of extruded AZ31 Mg alloy. Trans Nonferrous Met Soc China 25(11):3604–3610

[5] Zhang H, Yang M, Hou M et al (2018) Effect of pre-existing $10\bar{1}2$ extension twins on mechanical properties, microstructure evolution and dynamic recrystallization of AZ31 Mg alloy during uniaxial compression. Mater Sci Eng A 744:456–470

[6] Cepeda-Jiménez C, Molina-Aldareguia J, Pérez-Prado M (2015) Origin of the twinning to slip transition with grain size refinement, with decreasing strain rate and with increasing temperature in magnesium. Acta Mater 88:232–244

[7] Cepeda-Jiménez C, Molina-Aldareguia J, Pérez-Prado M (2015) Effect of grain size on slip activity in pure magnesium polycrystals. Acta Mater 84:443–456

[8] Mathis K, Čapek J, Clausen B, Krajňák T, Nagarajan D (2015) Investigation of the dependence of deformation mechanisms on solute content in polycrystalline Mg–Al magnesium alloys by neutron diffraction and acoustic emission. J Alloys Compd 642:185–191

[9] Vargas M, Lathabai S, Uggowitzer PJ et al (2017) Microstructure, crystallographic texture and mechanical behaviour of friction stir processed Mg-Zn-Ca-Zr alloy ZKX50. Mater Sci Eng A 685:253–264

[10] Wang L, Huang G, Quan Q, Bassani P et al (2014) The effect of twinning and detwinning on the mechanical property of AZ31 extruded magnesium alloy during strain-path changes. Mater Des 63:177–184

[11] Fan H, Aubry S, Arsenlis A, El-Awady JA (2016) Grain size effects on dislocation and twinning mediated plasticity in magnesium. Scr Mater 112:50–53

[12] Li J, Xu W, Wu X, Ding H, Xia K (2011) Effects of grain size on compressive behaviour in ultrafine grained pure Mg processed by equal channel angular pressing at room temperature. Mater Sci Eng A 528:5993–5998

[13] Figueiredo RB, Poggiali FS, Silva CL (2016) The influence of grain size and strain rate on the mechanical behavior of pure magnesium. J Mater Sci 51:3013–3024. https://doi.org/10.1007/s10853-015-9612-x

[14] Choi H, Kim Y, Shin J, Bae D (2010) Deformation behavior of magnesium in the grain size spectrum from nano-to micrometer. Mater Sci Eng A 527:1565–1570

[15] Lapovok R, Thomson P, Cottam R, Estrin Y (2005) The effect of grain refinement by warm equal channel angular extrusion on room temperature twinning in magnesium alloy ZK60. J Mater Sci 40:1699–1708. https://doi.org/10.1007/s10853-005-0672-1

[16] Chino Y, Kimura K, Mabuchi M (2008) Twinning behavior and deformation mechanisms of extruded AZ31 Mg alloy. Mater Sci Eng A 486:481–488

[17] Meyers M, Vöhringer O, Lubarda V (2001) The onset of twinning in metals: a constitutive description. Acta Mater 49:4025–4039

[18] Song B, Guo N, Liu T, Yang Q (2014) Improvement of formability and mechanical properties of magnesium alloys via pre-twinning: a review. Mater Des 62:352–360

[19] He J, Liu T, Xu S, Zhang Y (2013) The effects of compressive pre-deformation on yield asymmetry in hot-extruded Mg–3Al–1Zn alloy. Mater Sci Eng A 579:1–8

[20] Fu H, Ge B, Xin Y, Wu R, Fernandez C, Huang J et al (2017) Achieving high strength and ductility in magnesium alloys via densely hierarchical double contraction nanotwins. Nano Lett 17:6117–6124

[21] Liu Z, Xin R, Wu X, Liu D, Liu Q (2018) Improvement in the strength of friction-stir-welded ZK60 alloys via post-weld compression and aging treatment. Mater Sci Eng A 712:493–501

[22] Huo Q, Xiao Z, Yang X, Ando D et al (2017) Enhanced fatigue properties of cast AZ80 Mg alloy processed by cyclic torsion and low-temperature annealing. Mater Sci Eng A 696:52–59

[23] Song B, Xin R, Chen G, Zhang X, Liu Q (2012) Improving tensile and compressive properties of magnesium alloy plates by pre-cold rolling. Scr Mater 66:1061–1064

[24] Guo N, Song B, Guo C, Xin R, Liu Q (2015) Improving tensile and compressive properties of magnesium alloy rods via a simple pre-torsion deformation. Mater Des 83:270–275

[25] Song B, Wang C, Guo N, Pan H, Xin R (2017) Improving tensile and compressive properties of an extruded AZ91 rod by the combined use of torsion deformation and aging treatment. Material 10:280

[26] Xin Y, Wang M, Zeng Z, Nie M, Liu Q (2012) Strengthening and toughening of magnesium alloy by {10–12} extension twins. Scr Mater 66:25–28

[27] Hong S, Park S, Lee C (2010) Enhancing the fatigue property of rolled AZ31 magnesium alloy by controlling {10–12} twinning-detwinning characteristics. J Mater Res 25:784–792

[28] Park S, Hong S, Lee C (2013) Enhanced stretch formability of rolled Mg–3Al–1Zn alloy at room temperature by initial {10–12} twins. Mater Sci Eng A 578:271–276

[29] Kim S, Yim C, Lee Y, Yoon J, Lee J (2014) Controlling the microstructure of magnesium alloy sheet during rolling. Mater Sci Eng A 596:216–221

[30] Wang L, Cao M, Cheng W, Zhang H et al (2018) Improved stretch formability of AZ31 magnesium thin sheet by induced {10–12} tension twins. J Metal 70:2321–2326

[31] Teng J, Gong X, Li Y, Nie Y (2018) Influence of aging on twin boundary strengthening in magnesium alloys. Mater Sci Eng A 715:137–143

[32] Ungar T, Ott S, Sanders P, Borbély A, Weertman J (1998) Dislocations, grain size and planar faults in nanostructured copper determined by high resolution X-ray diffraction and a new procedure of peak profile analysis. Acta Mater 46:3693–3699

[33] Ribárik G, Ungár T (2010) Characterization of the microstructure in random and textured polycrystals and single crystals by diffraction line profile analysis. Mater Sci Eng A 528:112–121

[34] Dragomir I, Ungár T (2002) Contrast factors of dislocations in the hexagonal crystal system. J Appl Crystal 35:556–564

[35] Kim S-H, Jo W-K, Hong W-H et al (2017) Microstructural evolution of extruded AZ31 alloy with bimodal structure during compression. Mater Sci Eng A 702:1–9

[36] Wang X, Jiang L, Zhang D, Beyerlein IJ et al (2018) Reversed compressive yield anisotropy in magnesium with microlaminated structure. Acta Mater 146:12–24

[37] Jiang F, Liao W (2017) Effect of pre-compression deformation on stress-strain behavior of AZ31 alloy. Foundry Technol 38:1295–1297

[38] Barnett M, Keshavarz Z, Beer A, Atwell D (2004) Influence of grain size on the compressive deformation of wrought Mg–3Al–1Zn. Acta Mater 52:5093–5103

[39] Lu L, Huang J, Fan D et al (2016) Anisotropic deformation of extruded magnesium alloy AZ31 under uniaxial compression: a study with simultaneous in situ synchrotron x-ray imaging and diffraction. Acta Mater 120:86–94

[40] Ghaderi A, Barnett MR (2011) Sensitivity of deformation twinning to grain size in titanium and magnesium. Acta Mater 59:7824–7839

[41] Xie K, Alam Z, Caffee A, Hemker K (2016) Pyramidal I slip in c-axis compressed Mg single crystals. Scr Mater 112:75–78

[42] Syed B, Geng J, Mishra R, Kumar K (2012) [0 0 0 1] Compression response at room temperature of single-crystal magnesium. Scr Mater 67:700–703

[43] Byer CM, Li B, Cao B, Ramesh K (2010) Microcompression of single-crystal magnesium. Scr Mater 62:536–539

[44] Hutchinson W, Barnett M (2010) Effective values of critical resolved shear stress for slip in polycrystalline magnesium and other HCP metals. Scr Mater 63:737–740

[45] Kamikawa N, Huang X, Tsuji N, Hansen N (2009) Strengthening mechanisms in nanostructured high-purity aluminium deformed to high strain and annealed. Acta Mater 57:4198–4208

[46] He S, Zeng X, Peng L et al (2017) Microstructure and strengthening mechanism of high strength Mg–10Gd–2Y–0.5 Zr alloy. J Alloys Compds 427:316–323

[47] Lavrentev F (1980) The type of dislocation interaction as the factor determining work hardening. Mater Sci Eng A 46:191–208

[48] Armstrong R, Codd I, Douthwaite R, Petch N (1962) The plastic deformation of polycrystalline aggregates. Philos Mag 7:45–58

[49] Kim W, Lee H, Yoo S, Park Y (2011) Texture and mechanical properties of ultrafine-grained Mg–3Al–1Zn alloy sheets prepared by high-ratio differential speed rolling. Mater Sci Eng A 528:874–879

[50] Homma T, Mendis C, Hono K, Kamado S (2010) Effect of Zr addition on the mechanical properties of as-extruded Mg–Zn–Ca–Zr alloys. Mater Sci Eng A 527:2356–2362

[51] Wang R, Mao P, Liu Y, Chen Y, Wang Z, Wang F, Zhou L, Liu Z (2019) Influence of pre-twinning on high strain rate compressive behavior of AZ31 Mg-alloys. Mater Sci Eng A 742:309–317